Electron Temperature Measurements with Multi-Colour SXR Ratio Diagnostics on LM26 Plasma Compressions

W. Henry Gould, Abetharan Antony, Calum MacDonald, Xiande Feng, Ching Pui Hung, and Filiberto Braglia.

generalfusion®

6th European Conference on Plasma Diagnostics, Prague, CZ, April 7-10, 2025. **Poster P1.44.**

henry.gould@generalfusion.com

General Fusion's Magnetized Target Fusion

General Fusion is developing Magnetized Target Fusion (MTF) as a practical means of producing deuterium-tritium fusion power. In General Fusion's technology, a spherical tokamak plasma target is formed by coaxial helicity injection (CHI) into a rotating liquid lithium flux conserver (liner) and mechanically compressed to fusion conditions [1]. The rotation of the liquid liner generates a cylindrical cavity into which the plasma is formed and stabilizes fluid instabilities during compression.

The mechanical compression is driven by high pressure gas and requires no superconducting magnets or high-power lasers. The short compression timescale (~40 ms at powerplant scale) and compressive heating remove the need for any auxiliary heating, fueling, or external current drive after formation.

Overcoming Barriers to Commercial Fusion

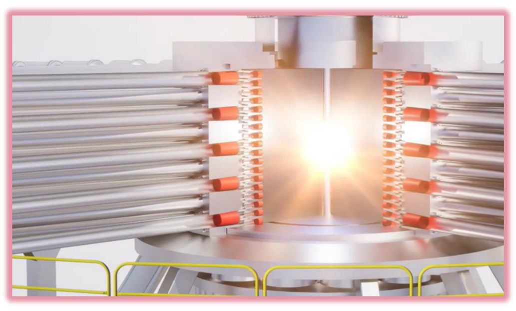

Durable Fusion Machine

Liquid metal wall compression technology absorbs neutrons and protects machine from fusion neutron flux

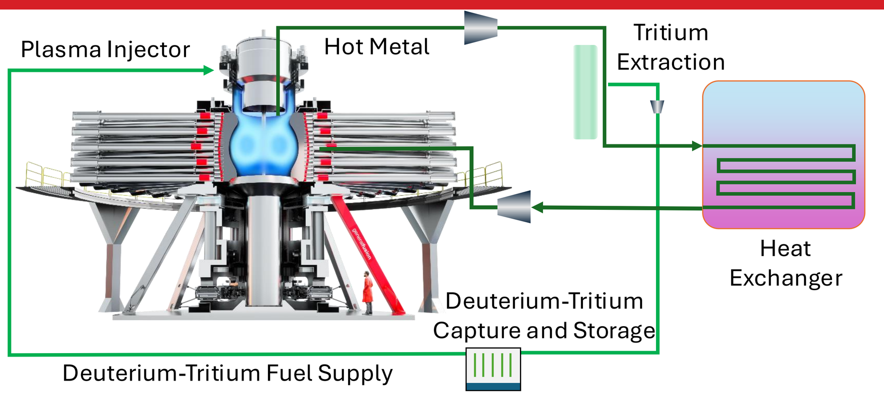

Sufficient Fuel Production

Liquid metal wall surrounding fusion plasma produces tritium fuel with a sustainable breeding ratio [2]

Simple Energy Extraction & Conversion

Liquid metal wall surrounding plasma absorbs neutron energy for simple conversion to electricity via steam turbine

Economical Fusion Power

Mechanical compression with liquid metal avoids the need for expensive magnets or targets, high-power lasers, and exotic/unavailable materials

Lawson Machine 26

LM26 is a large-scale MTF demonstration machine designed to achieve 1 keV, 10 keV, and ultimately, scientific breakeven equivalent (100% Lawson). A spherical tokamak is formed in a cylindrical target chamber with a solid lithium liner. Toroidal magnetic coils are pulsed, inducing compression of the lithium liner and plasma. Designed, assembled, and operational within 16 months of project launch, a preliminary variant of LM26 completed construction in Feb. 2025. It is designed to demonstrate ~1.5X temperature gain. The duration of compression is ~4 ms.

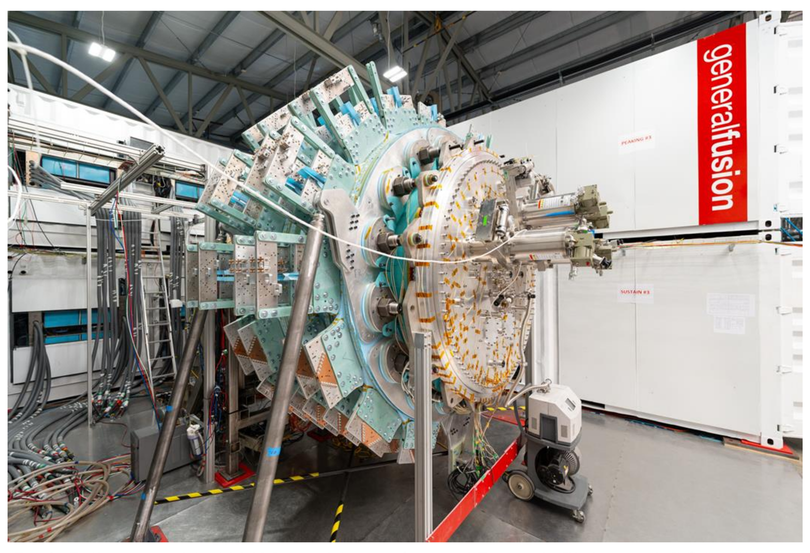

Fig 1. Fully assembled LM26 machine at General Fusion's Richmond, BC facility in February, 2025.

Table 1. Expected electron temperature and density at pre- and peak compression of the 1 keV and 10 keV variants.

	Pre-compression	Peak Compression (1keV variant)	Peak Compression (10keV variant)
$T_e(keV)$	$0.3 - 0.6$	$0.7 - 1$	10
$n_e(m^{-3})$	2×10^{19}	6×10^{20}	1.7×10^{22}

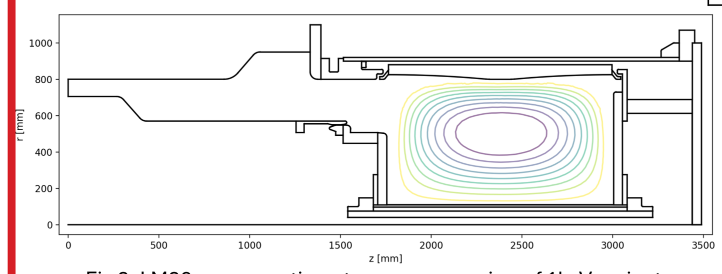

Fig 2. LM26 cross-section at pre-compression of 1keV variant.

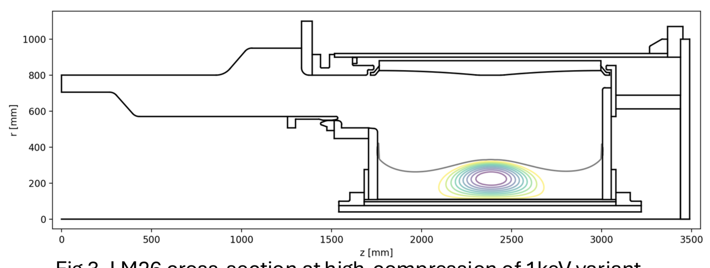

Fig 3. LM26 cross-section at high-compression of 1keV variant.

Principle of Diagnostic

The AXUV electron temperature method infers T_e using the ratio of soft X-ray (SXR) radiation incident on thick- and thin- filtered photodiodes [3], with cutoff energies in the SXR. The detected, filtered bremsstrahlung emissivity follows Eqn 1. The measured plasma brightness of a filtered diode follows Eqn 2. For two filters of the same material viewing a plasma with uniform T_e and n_e, the ratio can be plotted as a monotonic function of T_e (Eqn 3). To account for shaped plasma profiles, a forward model method was used. By assuming T_e and n_e profiles to be parabolic (e.g. Eqn 4 for T_e profile), synthetic ratios can be generated for each parameter combination (Fig. 4).

$$\epsilon_f(r,t) = CZ_{eff}\frac{n_e^2(r,t)}{\sqrt{T_e(r,t)}}\int_E dEA(E)T_f(E)\exp\left[-\frac{E}{T_e(r,t)}\right] \quad [1]$$

$$f_L(t) = \int_L \epsilon(L,t)dL \quad [2]$$

$$R(T_e) = \frac{\int_E e^{-\frac{E}{T_e}}T_{f,j}(E)dE}{\int_E e^{-\frac{E}{T_e}}T_{f,k}(E)dE} \quad [3]$$

$$T_e(r) = T_e(0)\left[1-\left(\frac{r}{a}\right)^2\right]^{\beta_{Te}} \quad [4]$$

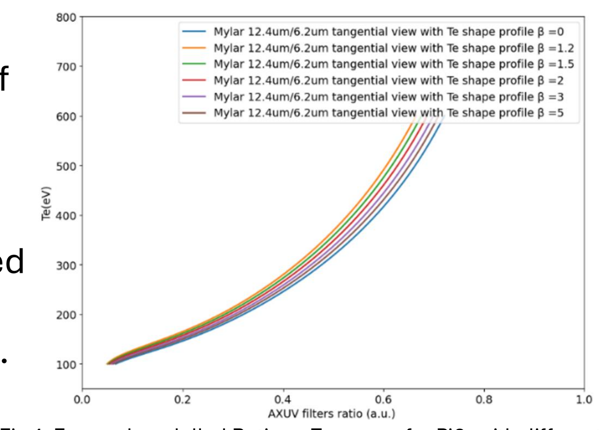

Fig 4. Forward modelled Ratio vs Te curves for Pi3, with different T_e shape parameters.

AXUV Analysis on PI3

On Plasma Injector 3 (PI3), General Fusion's former plasma device, T_e from AXUV did not match Thomson Scattering (TS) above ~350 eV. The initial variant of LM26 has no TS, so with the same AXUV Te, plasma heating would not be measurable.

Hypothesis: line radiation from metal impurities.

Approach: AXUV calculations were re-run assuming a set of impurities and various concentrations using FLYCHK [4] emissivity models. A dual annealing optimization was used to find the concentrations that minimized the difference between AXUV Te and TS Te. Table 2 shows the impurity configuration that best resolves the discrepancy.

Fig 5. General Fusion's PI3 plasma injector, now integrated into LM26.

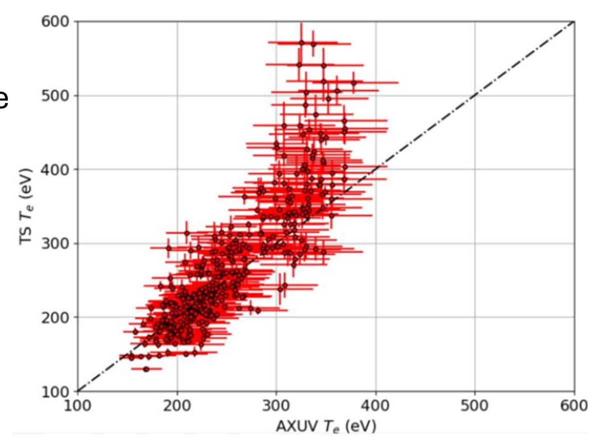

Fig 6. AXUV vs TS Te on Pi3, for 21/6 um ratio.

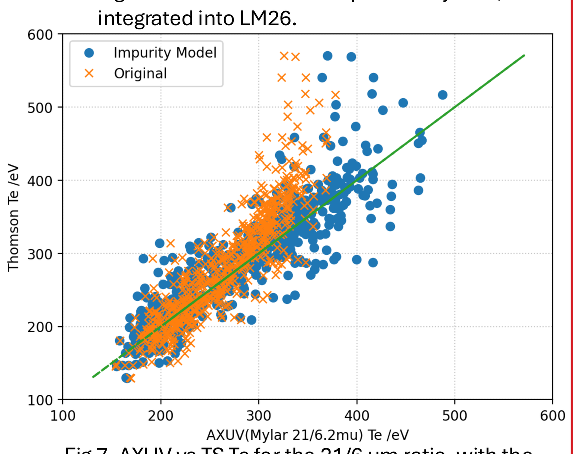

Fig 7. AXUV vs TS Te for the 21/6 um ratio, with the brems-only and best impurity config radiation model.

Sensitivity Analysis: a profile likelihood method. For a range of fixed concentrations for a given impurity, calcs are re-run. Determination of concentration confidence intervals is a work in progress.

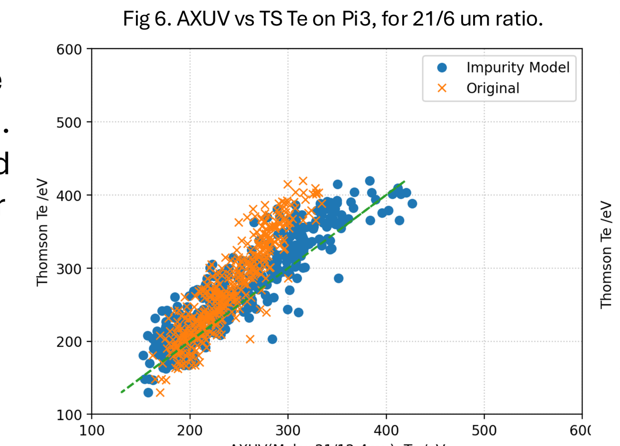

Fig 8. AXUV vs TS Te for the 12/6 um ratio, with the brems-only and best impurity config radiation model.

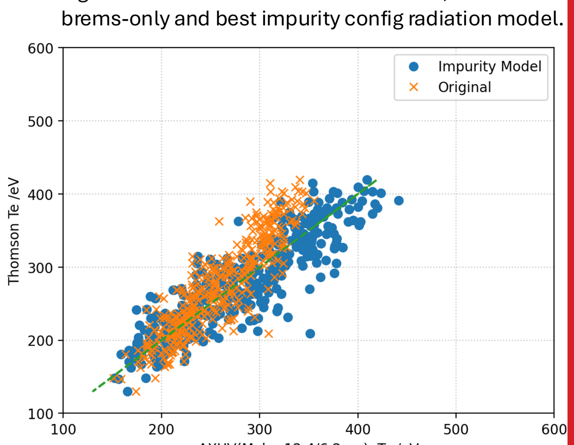

Fig 9. AXUV vs TS Te for the 21/12 um ratio, with the brems-only and best impurity config radiation model.

Table 2. The impurity concentrations that result in the best matching of AXUV and TS Te on PI3.

Element	Fractional Concentration
Deuterium	9.9×10^{-1}
Lithium	1.0×10^{-2}
Carbon	3.0×10^{-4}
Nitrogen	3.2×10^{-5}
Oxygen	4.0×10^{-4}
Aluminum	7.5×10^{-5}
Iron	5.7×10^{-7}
Tungsten	2.4×10^{-5}

Assumptions checks: a) linear scaling of emissivities between concentrations is valid, as needed for optimization, b) non-local thermal equilibrium steady state is valid for average ionization <20. High ionization states of Fe, W not-steady state. Implications of this is a work in progress.

Limitations: a) degenerate solutions may exist, b) impurity configuration for PI3 may not work for LM26.

Application to LM26: Need impurity configuration-informed assumption. Cannot perform same analysis without TS. Need Silicon Drift Detector [5] to measure spectrum in SXR.

Physics Design

Filter Criteria

Opted for same filters as PI3 (25 um, 13 um, 6 um Mylar with 0.1um of aluminum), designed to filter out carbon, nitrogen and oxygen. Ratio vs T_e curves shown in Fig 10. Considering future modification to have variable sensitivity of T_e to ratio over T_e range. Example using 0.4 um silver foil shown in Fig 11.

Compression Design Constraints

i) Diagnostic ports on cavity wall get eclipsed by liner. ii) T_e and n_e will increase significantly, causing large dynamic range in bremsstrahlung emission ($\propto n_e{}^2$).

AXUV A and B:

- Pre- and early compression
- Three filtered diodes, one unfiltered for proxy total radiated power measurement

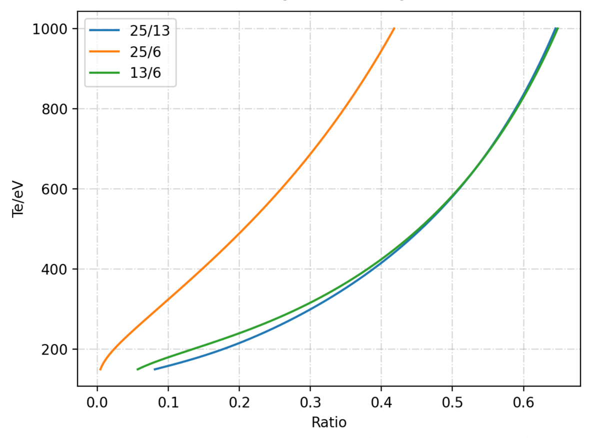

Fig 10. Ratio vs Te curves for LM26 filters (25um, 13um, 6um Mylar with 0.1um Al), according to Eqn 3.

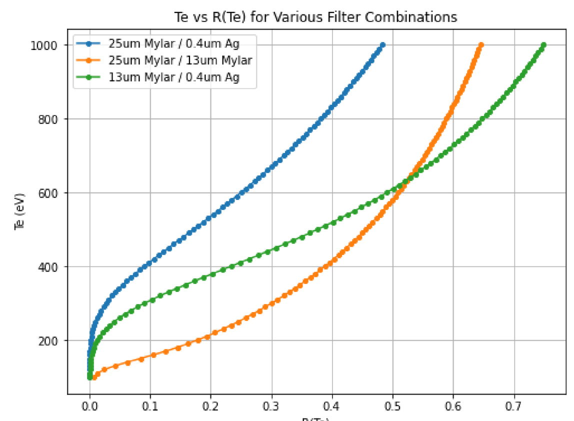

Fig 11. Ratio vs Te curves for potential modification of filters (25um, 13um, Mylar with 0.1um Al, and 0.4um Silver), according to Eqn 3.

AXUV C and D:

- High/peak compression core and pre-compression edge measurement
- One low-gain, narrow view cone, thick filter channel (13 um, 25 um)
- One high-gain, wide view cone, thin filter channel (6 um, 13 um)

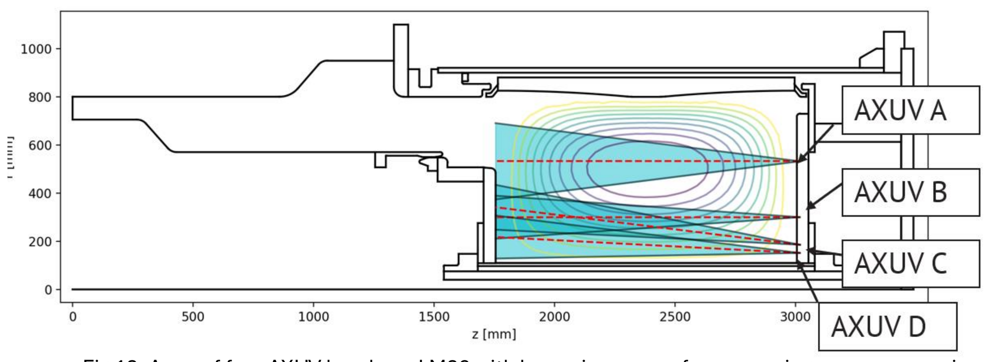

Fig 12. Array of four AXUV heads on LM26 with large view cones for measuring pre-compression.

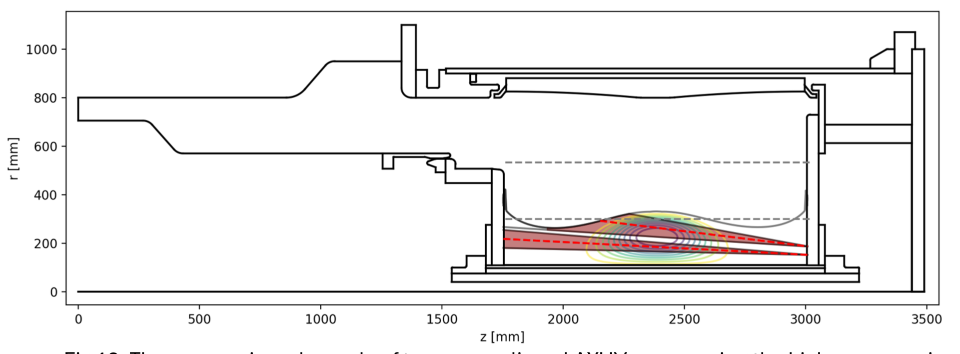

Fig 13. The narrow view channels of two non-eclipsed AXUVs, measuring the high compression plasma.

Analysis Method

Compression Constraint: Plasma shifts radially inwards with compression, plasma profile along line of sight changes.

Bayesian Reconstruction: General Fusion has an in-house magnetic and density reconstruction [6] using Bayes' theorem (Eqn 5) to find a probability distribution over Grad-Shafranov (GS) equilibrium states and n_e profiles. The forward model calculates diode signals from possible plasma states, using bremsstrahlung-only and impurity configuration-informed assumptions. The noise model includes filter transmission and measurement uncertainty.

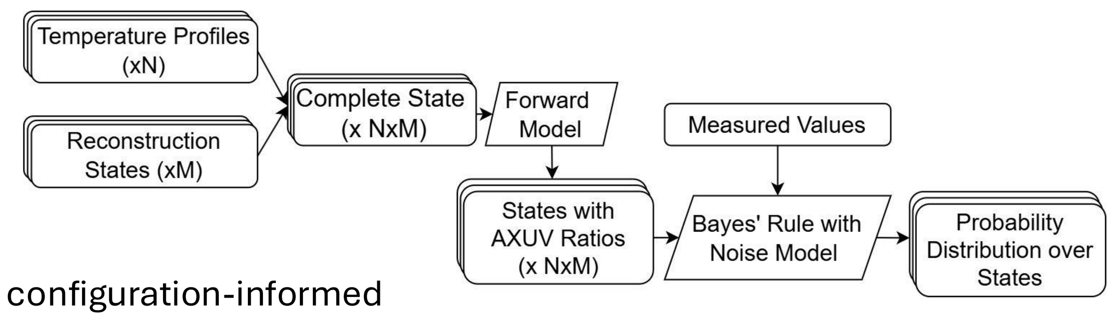

Fig 14. Flow chart of the AXUV Te reconstruction method on LM26.

Bayes' Rule:

A – plasma state params (GS state, n_e & T_e profiles); **m** – measurements; **P(A)** – prior likelihood of plasma state params; **P(m|A)** – likelihood of measuring ratios given state (forward model and noise model); **P(m)** – the prior likelihood of measured values

$$P(A|m) = \frac{P(m|A)P(A)}{P(m)} \quad [5]$$

Method:

1. Load results of density and magnetic reconstruction for each compression time slice
2. Assume key physics parameters (Z_{eff}, impurity mixture, recombination factor)
3. Generate synthetic diode signals for specified range of T_e profile params ($T_e(0), \beta_{Te}$)
4. Compare measured AXUV ratios to synthetic ratios using Bayes' rule and noise model to determine posterior distribution over the electron temperature profile

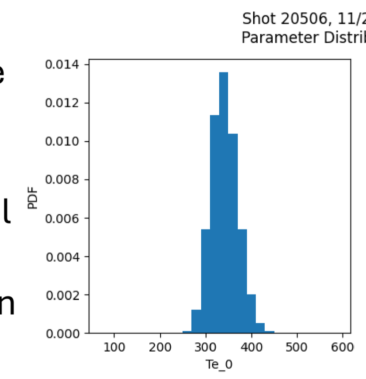

Outputs: a) Measurement tableau plots (Fig 15), b) forward model parameter distribution plots (Fig 16), c) stats of posterior distribution of Te profiles.

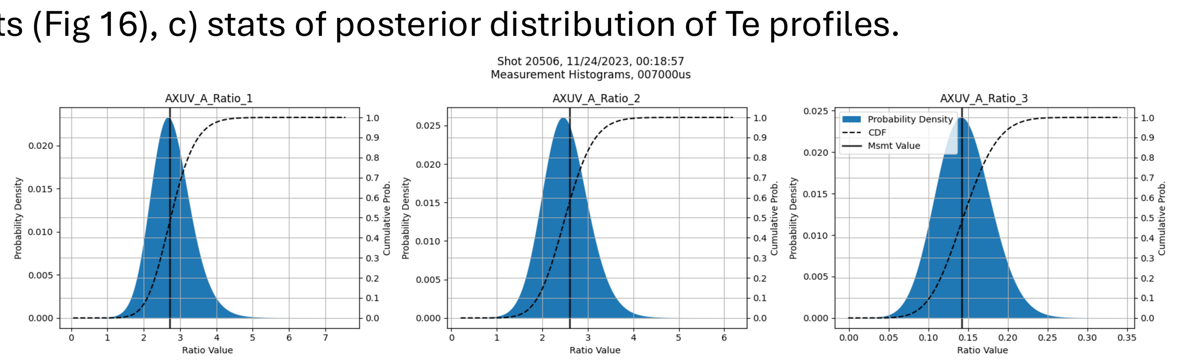

Fig 15. Measurement histograms for Pi3 showing the PDF of measured ratios (blue) for the posterior plasma state, the measured ratio (solid black) and the CDF (dotted black).

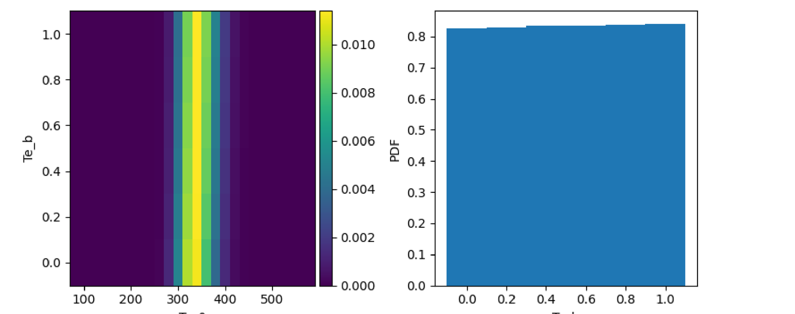

Fig 16. Forward model parameter distributions for test run on Pi3, including: i) PDF of core T_e, ii) PDF of β_{Te}, and iii) a 2D PDF heat map of both params, to show covariance.

Calibration

Filter transmission:

Filter transmission uncertainty currently based on manufacturer thickness tolerance. To calibrate transmission, use Amptek Mini-X2 X-Ray source (5-10 kV operation, silver anode) [7] incident on a Silicon Drift Detector (SDD) to measure SXR spectrum. Filter then placed in front of SDD to measure filtered spectrum. Filtered/unfiltered spectra are divided to calculate the transmission function (Eqn 6).

Diode Responsivity/Internal Head Geometry:

Currently assume constant diode responsivity in SXR, identical head geometry for each diode in ratio. Mount unfiltered AXUV head in front of filtered source to determine correction. Account for vignetting effects by rotating head and repeating.

$$T_f(E) = \frac{I_{f,filtered}(E)}{I_{unfiltered}(E)} \quad [6]$$

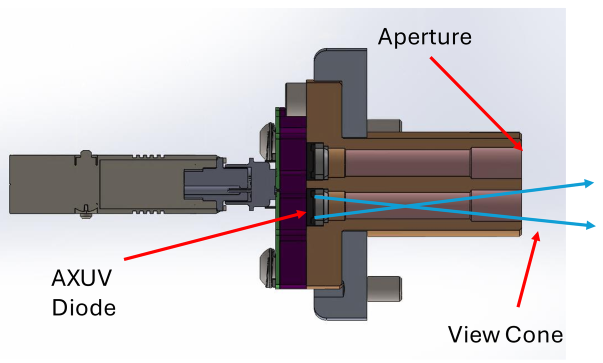

Fig 17. Cross section of AXUV diagnostic head CAD model.

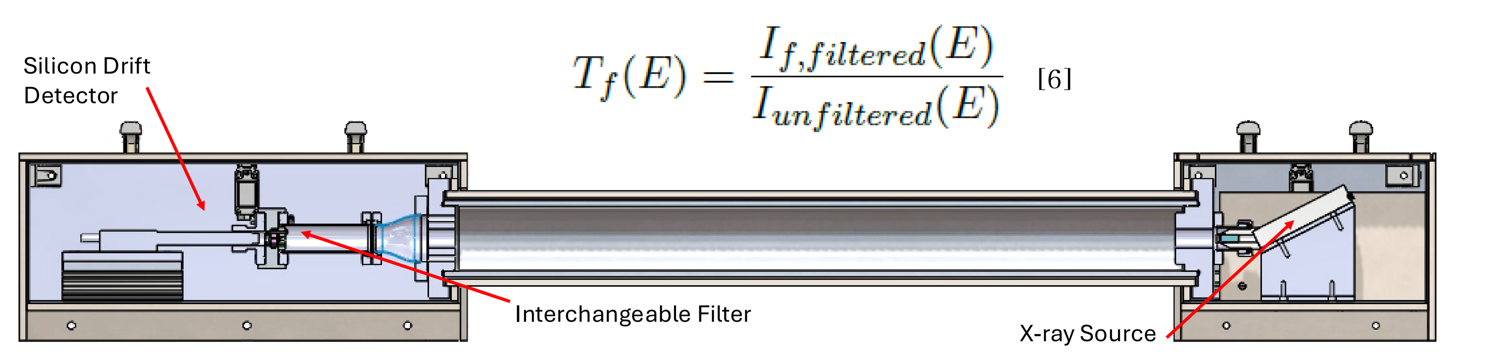

Fig 18. Cross section of X-ray calibration jig CAD model, in the filter transmission calibration setup.

Further Work

- Use plasma SXR spectrum measured by SDD to identify metal line radiation and inform impurity configuration assumption.
- Consider filtering the 4th diode to better constrain spectrum.

The authors would like to acknowledge the contributions of the General Fusion team who helped make this work possible.

References

[1] Laberge, Michel. "Magnetized target fusion with a spherical tokamak." *Journal of Fusion Energy* 38.1 (2019): 199-203.
[2] Eade, Tim, et al. "General Fusion TBR Analysis." *Report by UK Atomic Energy Authority* (2024) posted to General Fusion Research Library
[3] Optodiode Corporation. "Axuv20hs1 photodiode data sheet." optodiode.com. Accessed Feb, 2025.
[4] Chung, H.-K. et al. "FLYCHK: generalized population kinetics and spectral model for rapid spectroscopic analysis for all elements". High Energy Density Physics 1.1 (2005).
[5] Amptek Inc. "Fast sdd ultra high performance silicon drift detector." amptek.com. Accessed: Feb, 2025.
[6] A. Froese, R. Zindler et al., "Bayesian Equilibrium Reconstruction for General Fusion Demonstration Plant," presented at the APS DPP meeting, Spokane, WA, Oct. 2022.
[7] Amptek Inc. "Mini-x2 x-ray tube." Amptek.com. Accessed: Feb. 2025.